-RESEARCH PAPER-

International Journal of Mining and Geo-Engineering

IJMGE

IJMGE 57-3 (2023) 335-341

DOI: 10.22059/IJMGE.2023.360336.595071

Incorporating Topographic Variations on Electrical Resistance Tomography

Reza Ghanati [a,*], Mahdi Fallahsafari [a]

[a] *Institute of Geophysics, University of Tehran, Tehran, Iran.*

Article History:

Received: 04 June 2023.

Revised: 23 July 2023.

Accepted: 14 August 2023.

ABSTRACT

Electrical resistance tomography (ERT) provides images of the electrical properties of subsurface materials leading to the distinction of different Earth's interior structures. The accuracy of electrical resistance imaging is strongly affected by the topographical variations so the lack of incorporation of topography information into the inversion process may produce erroneous anomalies in the resistivity section. Owing to the significance of the topography effects on the resistivity measurements, we use the Schwarz-Christoffel transformation approach to incorporate the irregular surface into the 2.5-dimensional forward solution in the framework of the finite difference method. This approach is implemented on synthetic cases to illustrate how the resistivity measurements are dependent on the topographic irregularities. Numerical experiments demonstrate that in the presence of topographic features between current and potential electrodes, the resistivity response does not reflect the realistic resistivity values of the subsurface even in the case of a homogeneous resistivity distribution.

Keywords: *Electrical resistance tomography, Finite difference, Forward modelling, Schwarz-Christoffel transformation, Topography.*

1. Introduction

Electrical resistance tomography (ERT) as a near-surface geophysical method is based on the direct current theory of electrical conduction which is widely utilized in a variety of subsurface detection problems, e.g., mineral deposit exploration, engineering and environmental surveys, and groundwater investigations [1, 2, 3, 4]. ERT method in the context of 2D and 3D measurements is carried out aimed at imaging subsurface lithology based on the electrical properties of natural Earth materials. In such multidimensional cases, a precise model of the earth's subsurface is highly dependent upon the forward calculation which is implemented inside of the inverse algorithm [5]. Even though an accurate forward and inverse solution is necessary to provide a reliable interpretation of resistivity data, the presence of topography may produce misleading subsurface anomalies. Hence, to distinguish the terrain-induced anomalies from subsurface anomalies, it is required to incorporate topography in the forward solver. According to the significance of the topographic variations in ERT data, in recent years, several studies have been done in the framework of different numerical methods. These attempts are categorized into two schemes known as topographic corrections and topographic modelling. The topographic corrections method attempts to eliminate topographic effects using the calculation of the apparent resistivity values due to a homogeneous earth model with incorporation of the observed topography and then multiplication of the ratio of the true resistivity to the calculated apparent resistivity values for the homogeneous earth with the field resistivity measurements. This approach is successful if the subsurface earth model is also homogeneous. The topography modeling method is directly included in the forward modeling process. Referring to the above calcification and with emphasis on the importance of accounting for surface irregularities to ensure valid interpretive models of resistivity and induced polarization measurement results, [6] proposed a linear correction method to reduce the topographic effect from ERT data collected along a line. [7] suggested a 3D ground correction algorithm based on the linear correction method. It was later shown by [8] that in complex subsurface media, the resistivity response may not be separated completely from the topography effect when using linear correction techniques such as those presented by [6]. [8] developed an algorithm for 2D resistivity inversion in which topography is incorporated into the modeling process. Further developments were reported by many other authors using the second method in the framework of finite difference and finite element numerical algorithms. The finite element method due to more flexibility to model both topography and possibly complex geometries has attracted further attention. For instance, [9] and [10] proposed finite element modeling including topography on distorted grids. [11], [12], and [13] developed an unstructured mesh generation with the corporation of topography using the finite element algorithm. [14] proposed a modification of the singularity removal approach to handle the surface topography. Their idea is based on utilizing the analytic solution defined for flat surface topography and uniform resistivity distribution models as the primary potential and modifying the free surface conditions for the computation of the secondary potential. In contrast to the finite element method which is widely used to simulate complex terrain tomography and substructures, there are very limited applications of the finite difference, despite being fast and memory efficient, in the forward solution in the presence of irregular terrain. For example, [15] provided a performance comparison between the finite difference and finite element methods to simulate topographic effects in the 2D resistivity forward modeling. They concluded that the results of the finite difference algorithm are comparable to the finite element method with computationally more efficient functionality. In addition [16] proposed the use of a finite difference forward solution with a triangular grid to include surface topography into the inverse solution. Following the conclusions drawn by [15], we take advantage of

* Corresponding author: *E-mail address:* rghanati@ut.ac.ir (R. Ghanati).

the finite difference method for 2.5D resistivity forward computation. In this contribution, we numerically deal with the topographic effects on resistivity forward response derived from different electrode configurations. To incorporate undulating surface topography, we apply an efficient mapping function known as the Schwarz-Christoffel transformation method for transferring the problem in the W-plane (the plane with undulating surface topography) to the Z-plane (the plane with flat surface topography) such that the problem is solved in the W-plane and at the end it is possible to return bo the W-plane again using inversion of the Schwarz–Christoffel conformal transformation. The Schwarz-Christoffel transformation is widely used in the field of fluid dynamics such as grid generation for computational fluid dynamics and nonlinear free-surface flow over uneven bottom topographies.

Despite recent improvements in various algorithms of 2D/3D forward and inverse modeling of electrical resistance imaging in the presence of topographical variation, it could be still an interesting research area for scholars interested in this issue. The advantage of this study compared to previous studies is to formulate the proposed transformation in detail with an emphasis on electrical resistance imaging which can be interesting to the geoscience community.

The rest of the paper is organized as follows. The 2.5-dimensional resistivity forward algorithm and a detailed formulation and solution of the proposed transformation function based on a numerical integration procedure are presented in section 2. In section 3, the topographic variations from simple to complex cases are taken into account for apparent resistivity values calculation. The conclusions are drawn in section 4.

2. Methodology

In this section, we first provide a very brief explanation of the 2.5D resistance forward computation. For further details about the finite difference solution of the Poisson's equation, readers are referred to [17] in which the forward solver is validated to some non-topography earth models by comparing them with the analytic solutions. Then, we extend a mapping function based on the Schwarz-Christoffel transformation. Applications of this approach are made to the solution of problems in fluid flow and electrostatic potential theory. In this contribution, the forward calculation and the Schwarz-Christoffel transformation codes are developed with MATLAB scripts.

2.1. 2.5D Direct current resistance forward solution

An initial and important step is to formulate and solve a 2.5D electrical resistivity forward modeling problem. The advantage of the 2.5D approach is that a physically realistic representation, involving full 3D electrical potential distribution is derived by solving several problems with a restricted 2D geometry in terms of several wavenumbers. In this way, the computational time is reduced compared to full 3D forward modeling. Computation of electrical resistivity forward responses is implemented using simulation of the current flow into the Earth's surface through solving the Poisson's equation using the finite difference approximation with the mixed boundary conditions proposed by [18]. One of the advantages of the finite-difference method over the other numerical methods is its well-known ability to quickly approximate the solutions for any arbitrary and complex substructures. The 3D distribution of electrical potential due to a point source $r_s(x_s.y_s.z_s)$ is expressed by the following governing equation:

$$\nabla\cdot\left[\frac{1}{\rho(x,y,z)}\nabla\varphi(x.y.z)\right]=-I\delta(x-x_s)\delta(y-y_s)\delta(z-z_s) \quad (1)$$

where $\rho(x,y,z)$ is the resistivity distribution, $\varphi(x.y.z)$ is the electrical potential in 3D space, I is the point current source on the surface of the earth, and δ indicates the impulse function and the source location. To account for the 3D source characteristic, we need to Fourier transform the partial differential equation (1) with respect to y, the strike direction, using the cosine transform:

$$\tilde{\varphi}(x.k_y.z)=\int_0^{\infty}\varphi(x.y.z)\cos(k_y y)\,dy \quad (2)$$

where $\tilde{\varphi}$ stands for the transformed potential in the wavenumber domain and k_y is the wavenumber with respect to y.

Applying the Fourier-cosine transformation to the 3D Poisson's equation (1), we get the equation:

$$\frac{\partial}{\partial x}\sigma(x.z)+\frac{\partial\tilde{\varphi}}{\partial x}+k_y^2\sigma(x.z)\tilde{\varphi}-\frac{\partial}{\partial z}\sigma(x.z)\frac{\partial\tilde{\varphi}}{\partial z}=-\frac{I}{2}\delta(x-x_s)\delta(z-z_s) \quad (3)$$

Equation (3) is numerically solved using rectangular or triangular mesh discretization produce. Having obtained discrete representations for the principle governing equations and boundary conditions at all cells, the transformed forward problem can be represented as a linear system of equations:

$$\boldsymbol{\Gamma}\tilde{\varphi}=\boldsymbol{\xi} \quad (4)$$

$\boldsymbol{\Gamma}$ indicates a real sparse five-band symmetric matrix and $\boldsymbol{\xi}$ displays the source vector. This equation has to be solved for the vector $\tilde{\varphi}$ containing the potentials for all existing nodes. By taking advantage of the sparsity of the matrix $\boldsymbol{\Gamma}$, it is possible to use direct methods that can be computationally efficient. The solution $\tilde{\varphi}$ is then transformed from the wavenumber domain to the spatial domain (i.e., x-z plane) following the procedure of [18] and based on the inverse cosine-Fourier transform,

$$\varphi(x.z)=\frac{2}{\pi}\int_0^{\infty}\tilde{\varphi}(x.k_y.z)\cos(k_y y)\,dK_y \quad (5)$$

2.2. Formulation of Schwarz-Christoffel transformation

To incorporate uneven surface topography, we utilize an efficient mapping function known as the Schwarz-Christoffel transformation method for transferring the problem in the plane with non-flat surface topography (say, W-plane) to the plane with flat surface topography (say, Z-plane) such that the solution process is implemented in the Z-plane and at the end it is possible to return back to the W-plane again using inversion of the Schwarz–Christoffel conformal transformation. We take advantage of the finite difference method for 2.5D resistivity forward computation due to its flexibility and less computational time and memory storage. In the finite difference method, each derivative is solved by approximating derivatives; therefore, it is simple to code, and advantageous to compute as well. In some cases, this method offers a more direct and easy approach to the numerical solution of partial differential equations compared to other techniques.

To have the Green's function valid in surface electrical resistivity surveying, it is essential to record the data on the flat earth's surface. Hence, this is a bottleneck for the numerical simulation by the finite difference on the non-flat earth's surface. This paper suggests a drastically efficient method for computing the distribution of electrical potential on the non-flat earth's surface. The solution is obtained by transforming the irregular surface to a flat surface using the SC transformation.

The SC transformation provides a formula for mapping of the half-plane onto a plane polygon. The solution of this problem is obtained by setting up a nonlinear system of equations. This subsection presents a detailed explanation of the SC transformation formulation and a flowchart of the algorithm implementation which may not be found in the geophysical literature.

The definition of the SC transformation which maps the X-axis and the upper half of the Z-plane (see Figure 1(a)) onto a given closed polygon and its interior in the W-plane (see Figure 1(b)) is given as [19, 20].

$$W=A\int_0^{z}(Z-x_1)^{-\alpha_1}\dots(Z-x_n)^{-\alpha_n}dZ+B \quad (6)$$

where A and B are complex constants, x_1 to x_n are the vertex image points in the Z-plane on the real axis , and the inequality relations $x_1<x_2<\cdots<x_n$ are taken as the constraints of the system. The parameters α_1 to α_n denote the corresponding vertex exterior angles measured in fractions of a half-circle (Figure 1).

The vertex points W_1 to W_n and the angles α_1 to α_n are definite, but their image points x_1 to x_n are variable. Now the problem can be written based on numerous pairs that satisfy the following relationship to

change contour integral of Equation (6) to a real integral as:

$$W_1 = (-1)^{-\alpha_1-\alpha_2\dots-\alpha_n} A \int_0^{x_1} |x_1 - x|^{-\alpha_1} |x_2 - x|^{-\alpha_2} \dots |x_n - x|^{-\alpha_n} dx + B \quad (7)$$

$$W_2 = W_1 + (-1)^{-\alpha_2\dots-\alpha_n} A \int_{x_1}^{x_2} |x - x_1|^{-\alpha_1} |x_2 - x|^{-\alpha_2} \dots |x_n - x|^{-\alpha_n} dx + B$$

Equation (7) is appropriately solved by the difference of the pair of vertices $|W_j - W_{j-1}|$ and $|W_{j-1} - W_{j-2}|$ as:

$$|W_j - W_{j-1}| = |A| \int_{x_{j-1}}^{x_j} \prod_{i=1}^{n} |x - x_i|^{-\alpha_i} dx \quad (8)$$

$$|W_{j-1} - W_{j-2}| = |A| \int_{x_{j-2}}^{x_{j-1}} \prod_{i=1}^{n} |x - x_i|^{-\alpha_i} dx \quad (9)$$

Then it may be possible to eliminate the constant A by the ratio of Equation (8) to Equation (9) to give:

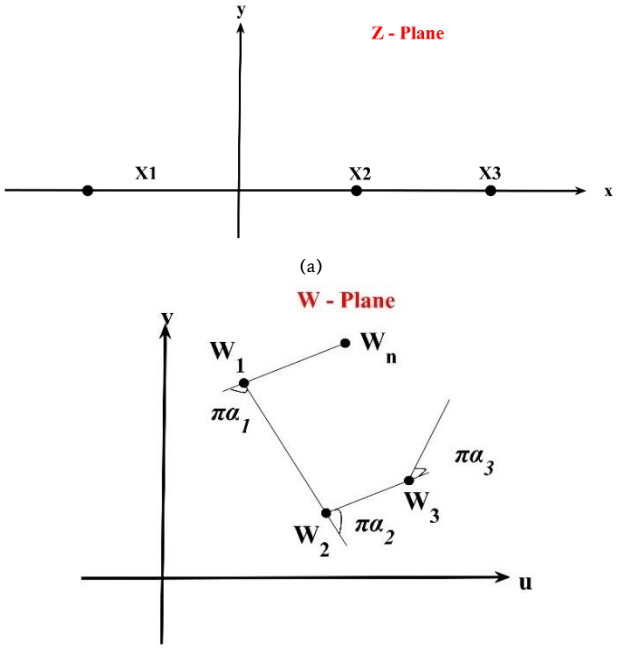

Figure 1. representation of mapping the X-axis and the upper half of the Z-plane onto a given closed polygon and its interior in the W-plane.

$$\frac{|W_{j-1}-W_{j-2}|}{|W_j-W_{j-1}|} \int_{x_{j-1}}^{x_j} \prod_{i=1}^{n} |x - x_i|^{-\alpha_i} dx - \int_{x_{j-2}}^{x_{j-1}} \prod_{i=1}^{n} |x - x_i|^{-\alpha_i} dx = 0 \quad (10)$$

Indicating the length ration of $|W_n - W_{n-1}|$ to $|W_2 - W_1|$ as $\lambda_2, \lambda_3, \dots, \lambda_n$; then we have:

$$\frac{|W_3-W_2|}{|W_2-W_1|} = \lambda_2, \ \frac{|W_4-W_3|}{|W_2-W_1|} = \lambda_3, \dots, \frac{|W_n-W_{n-1}|}{|W_2-W_1|} = \lambda_{n-1}, \quad (11)$$

We take the following values to fix the relations between the Z-plane and the W-plane; $x_1 = 0$ is maped to W_1 so that $B = W_1$ and $x_2 = 1$ is correspondent to W_2.

Substituting Equation 8 into Equation 11 gives the following system with:

$$\begin{aligned} &I_2(x_3, x_4, \dots, x_n) = \lambda_2 I_1(x_3, x_4, \dots, x_n), \\ &I_3(x_3, x_4, \dots, x_n) = \lambda_3 I_1(x_3, x_4, \dots, x_n), \\ &\vdots \\ &I_{n-1}(x_3, x_4, \dots, x_n) = \lambda_{n-1} I_1(x_3, x_4, \dots, x_n), \end{aligned} \quad (12)$$

Where:

$$I_k = (-1)^{-\alpha_1-\alpha_2\dots-\alpha_n} \int_{x_k}^{x_{k+1}} |x_1 - x|^{-\alpha_1} |x_2 - x|^{-\alpha_2} \dots |x_n - x|^{-\alpha_n} dx, \quad (13)$$

The above system is nonlinear and it must be solved using iterative methods. We need to find ways to match coefficients by rewriting Equation 12 as [21]

$$\begin{aligned} &F_2(x_3, x_4, \dots, x_n) = I_2 - \lambda_2 I_1 = 0, \\ &F_3(x_3, x_4, \dots, x_n) = I_3 - \lambda_3 I_1 = 0, \\ &\vdots \\ &F_{n-1}(x_3, x_4, \dots, x_n) = I_{n-1} - \lambda_{n-1} I_1 = 0, \end{aligned} \quad (14)$$

Then it can be easily calculated the jacobian matrix.

$$[J] = \begin{bmatrix} \frac{\partial I_2}{\partial x_3} & \frac{\partial I_2}{\partial x_4} & \dots & \frac{\partial I_2}{\partial x_n} \\ \frac{\partial I_3}{\partial x_3} & \frac{\partial I_3}{\partial x_4} & \dots & \frac{\partial I_3}{\partial x_n} \\ \vdots & \vdots & & \vdots \\ \frac{\partial I_{n-1}}{\partial x_3} & \frac{\partial I_{n-1}}{\partial x_4} & \dots & \frac{\partial I_{n-1}}{\partial x_n} \end{bmatrix} - \begin{bmatrix} \lambda_2 \\ \lambda_3 \\ \vdots \\ \lambda_{n-1} \end{bmatrix} \begin{bmatrix} \frac{\partial I_1}{\partial x_3} \\ \frac{\partial I_1}{\partial x_4} \\ \vdots \\ \frac{\partial I_1}{\partial x_n} \end{bmatrix}^T \quad (15)$$

Estimated values of x_i are determined from the inversion process. However, each evaluation of x_i requires calculation of $\frac{\partial I_k}{\partial x_i}$. Therefore, a five-point Lagrange differential formula can be used to evaluate the derivatives $\partial I_k / \partial x_i$. We declare five points at the vicinity of x_i such that:

$$x_i - 2h < x_i - h < x_i < x_i + h < x_i + 2h,$$

where h is the length of a segment, and from our experiment, we set $h = 0.01$

$$\frac{\partial I_k}{\partial x_i} \approx [I_k(x_i - 2h) - 8I_k(x_i - h) + 8I_k(x_i + h) - I_k(x_i + 2h)]/12h \quad (16)$$

Where:

$$I_k(x_i \pm nh) = I_k(x_1, x_2, \dots, x_i, \dots, x_n)|_{x_i = x_i \pm nh}, \quad n = 1,2. \quad (17)$$

Finally, A can be calculated by derivative of Equation (6) in terms of Z. In other words, all the available variables are obtained in the SC transformation. Algorithm 1 summarizes the SC transformation.

Algorithm 1. Schwarz-Cristoffel transformation

1. Inputs: vertex coordinate: $W_i, \quad i = 1, 2, \dots, n$
2. Outputs: A, B, x_i
3. Compute vertex exterior angles $\alpha_i \quad i = 1, 2, \dots, n$
4. Calculate λ using $\lambda_i = \frac{|W_{i+1}-W_i|}{|W_2-W_1|}, i = 2,3, \dots, n-1$
5. Put an initial value for x_i
6. Compute $I(x_i)$: $I_n = (-1)^{-\alpha_1-\alpha_2\dots-\alpha_n} \int_{x_n}^{x_{n+1}} |x_1 - x|^{-\alpha_1} |x_2 - x|^{-\alpha_2} \dots |x_n - x|^{-\alpha_n} dx, \ i = 1,2, \dots, n-1$
7. Compute $F(x_i)$: $F_i(x_3, x_4, \dots, x_n) = I_i - \lambda_i I_1 = 0, \ i = 2,3, \dots, n-1$
8. Construct Jacobian matrix using Equation 15
9. Calculate x_i by iterative constrained inversion technique
10. Set $B = W_1$
11. Compute $A = \frac{W}{\int_0^Z (Z-x_1)^{-\alpha_1} \dots (Z-x_n)^{-\alpha_n} dZ + B}$

In addition, we can return back to the Z-plane again using inversion of the SC conformal transformation.

3. Numerical examples

In this section, the results from three synthetic tests of forward modeling aimed at dealing with the effect of topography on forward solutions are presented. The synthetic models are simulated using the most common configurations (e.g. collinear Dipole-Dipole, Pole-Dipole, and Wenner arrays) with different surface topographies and subsurface resistivity distribution. All synthetic models share the same discretization parameters. Figure 2 shows different parts of the incorporation of surface topography into ERT forward modeling.

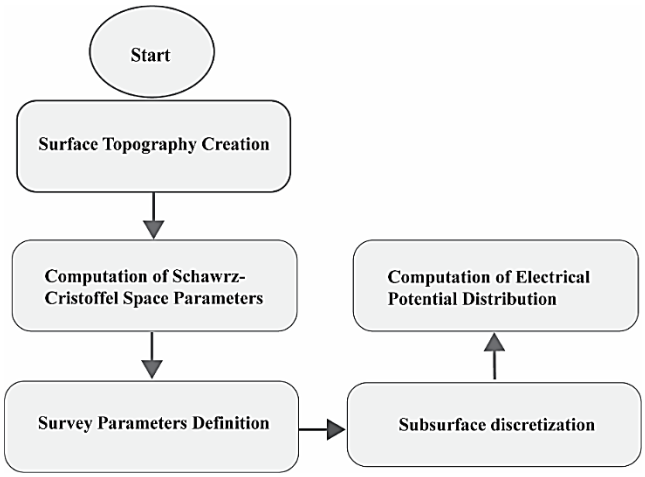

Figure 2. Flowchart of incorporation of surface topography into ERT forward modelling.

Model 1

The first example includes a homogeneous earth model with the resistivity value of 100 $\Omega.m$. The apparent resistivity responses of the simulated model are computed assuming a multi-electrode system with 40 electrodes and fixed electrode spacing of 2 m up to 8 levels ($n = 1 - 8$, where n displays the number of receiver-transmitter dipole separation) leading to a total of 132 measurements. The forward responses are computed in the presence of the topographical effects including a symmetric hill along the survey line.

Figure 3 shows the results of the forward solution in terms of different electrode arrays. It is observed that the apparent resistivity section beneath the area of the valley and hill exhibits conductive and resistive anomalies, despite the homogeneous earth model, depending on the type of electrode configuration. In the case of Dipole-Dipole and Pole-Dipole arrays, this behavior is because of concentrating the current flow in the valley and diverging the current flow in the hill leading to, respectively, diverging (i.e., high resistivity values) and converging (i.e., low resistivity values) the equipotential surfaces.

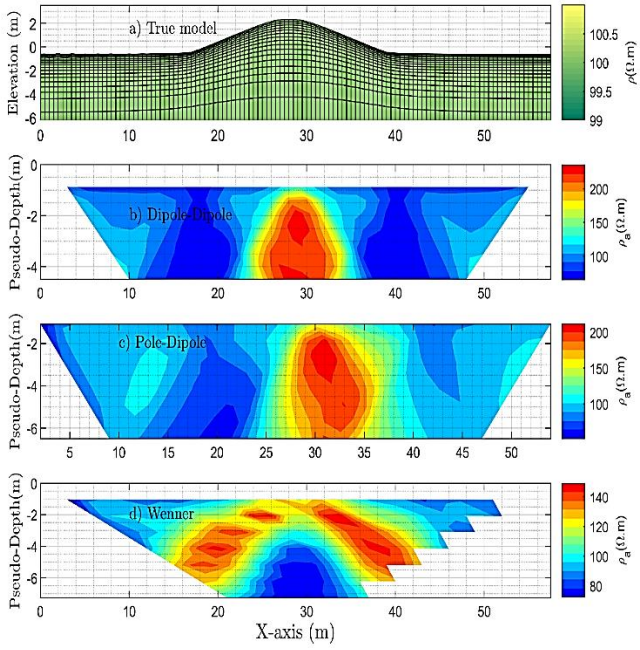

Figure 3. Apparent resistivity pseudo-sections computed by the proposed SC transformation method for Model 1 presented in panel (a) using different electrode arrays (panels b to d). The model is homogeneous at 100 $\Omega.m$.

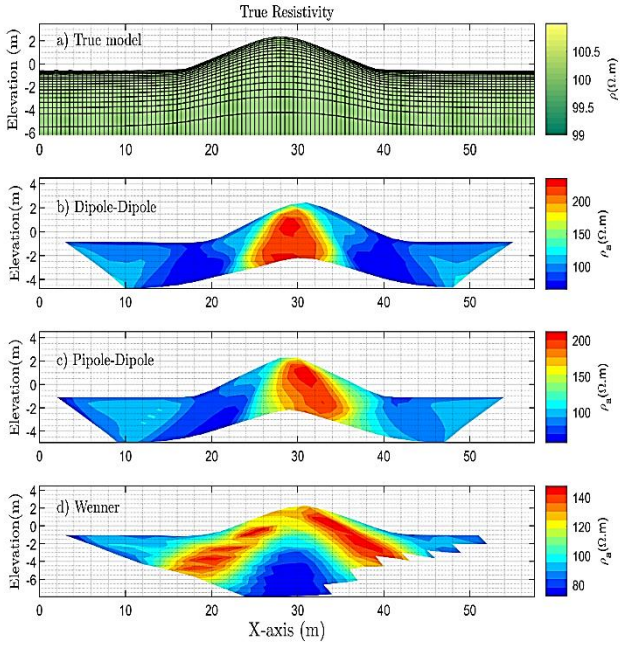

Figure 4. Apparent resistivity pseudo-sections with the surface nodes shifted up or down using the inverse SC transformation method for Model 1 presented in panel (a) using different electrode arrays. The model is homogeneous at 100 Ω.m.

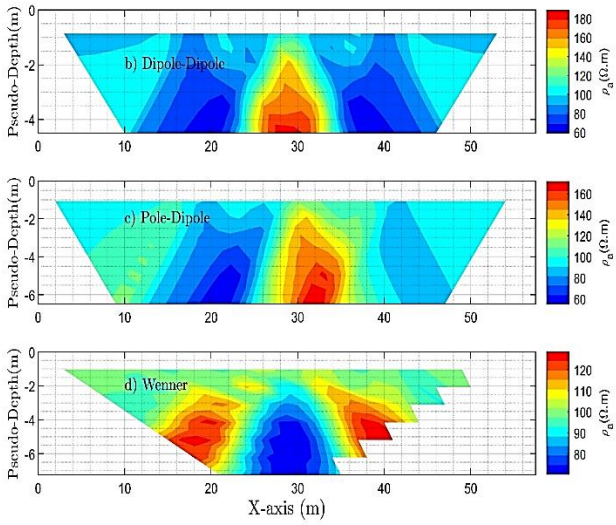

Figure 5. Apparent resistivity pseudo-sections computed by the commercial software RES2DMOD for Model 1 presented in panel (a) using different electrode arrays (panels b to d). The model is homogeneous at 100 Ω.m.

It is evident that the Wenner array produces an effect opposite to those of the Dipole-Dipole and Pole-Dipole resistivity data. Besides, the apparent resistivity sections, due to the irregular surface, are accompanied by low and high resistivity zones on the flanks, respectively, in Dipole-Dipole (or Pole-Dipole) and Wenner arrays. To better illustrate the topographical variations on the apparent resistivity distribution, we also show the pseudo-sections with the surface nodes shifted up or down using the inverse SC transformation method in Figure 4. From Figure 4, one can see that the geometry of resistivity pseudo-sections is modified while the magnitude of physical properties is preserved. Whereas there is no analytic solution, a comparison of the values of the apparent resistivity computed by commercial software (RES2DMOD ver. 3.03.06; [22]) is provided in Figure 5. Visually comparing the resulting pseudo-sections, it is evident that there is a trivial difference between the apparent resistivity contours obtained from our algorithm and the commercial software.

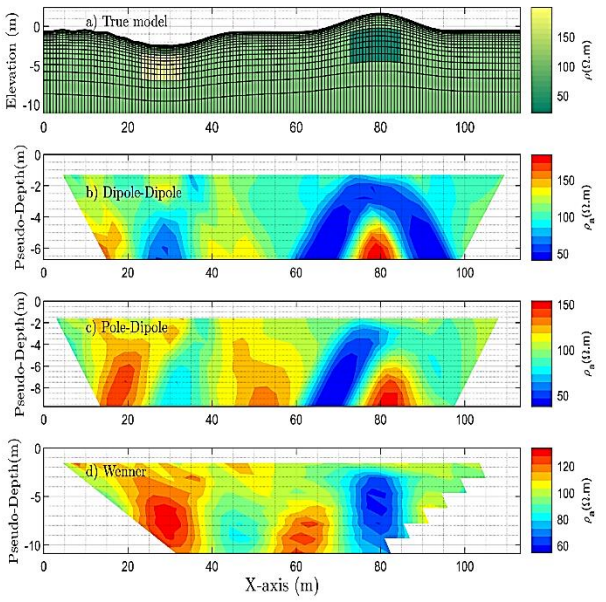

Figure 6. Apparent resistivity pseudo-sections computed by the proposed SC transformation method for Model 2 presented in panel (a) using different electrode arrays (panels b to d). The model consists of two blocks with resistivity values of 200 and 20 Ω.m buried in a 100 Ω.m background.

Model 2

The second synthetic model consists of three different mediums in terms of resistivity distribution. The two blocks with the resistivity of 200 $\Omega.m$ (left block) and 20 $\Omega.m$ (right block) are embedded in a 100 $\Omega.m$ background. In addition, the surface topographical effects consist of a valley and a hill with a conductive anomaly along the survey line. The resistivity measurements are conducted from position 0 up to 115 m using 48 electrodes at the surface with a fixed electrode spacing of 3 m. Apparent resistivity values from three electrode arrays are computed up to 8 levels. Figure 6 displays the resulting forward solution in the presence of topography. It is seen from the pseudo-sections that the effect of the conductive and resistive anomalies on the resistivity values is masked by the presence of undulating terrain tomography so that no discernible features of the subsurface anomalies are resolved. Due to the fact that current flow diverges below the area of the valley and converge below the hill, the pseudo-sections are accompanied by conductive and resistive anomalies beneath the valley and hill area, respectively. The results of inverse SC transformation aimed at modifying the geometry of resistivity pseudo-sections in the presence of topography impacts are represented in Figure 7.

Model 3

To better evaluate the proposed mapping function in the presence of more complex surface topography, the last example includes a longer survey line with different topographical variations. The apparent electrical resistivity responses of the synthetic model are simulated using three configurations from position 0 up to 130 m with fixed electrode spacings of 3 m up to 8 levels. Figures 8 indicate the resistivity pseudo-sections derived from the third synthetic model.

The same as the previous examples, the undulated surface leads to artificial conductive and resistive substructures whereas on a flat surface without topography such anomalies are highly unlikely to be significant. It is evident that, according to the electrode array, the inline Dipole-Dipole and Pole-Dipole arrays create high and low apparent resistivity anomalies, respectively, below the area of the hill and valley while the Wenner measurements lead to the results opposite to those of the Dipole-Dipole and Pole-Dipole surveys. Comparing the resulting forward responses of three synthetic earth models, one can see that by increasing the complexity of surface topography further terrain-induced anomalies may appear in electrical resistance tomography measurements. We also represent the apparent resistivity distribution with the surface nodes shifted up or down using the inversion of the SC transformation method in terms of different electrode arrays in Figure 9.

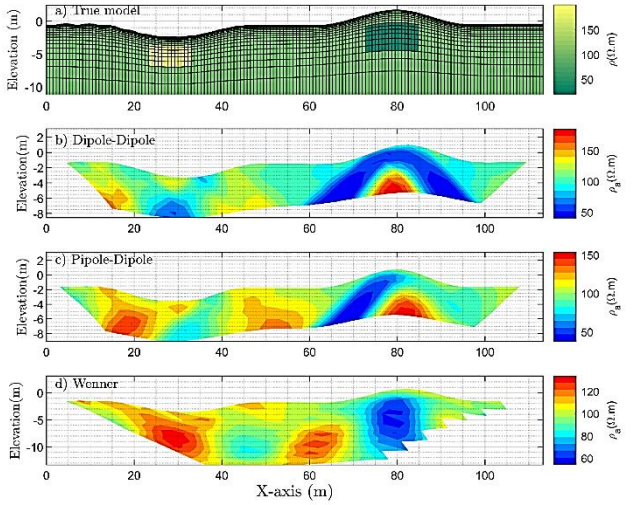

Figure 7. Apparent resistivity pseudo-sections computed by the commercial software RES2DMOD for Model 2 presented in panel (a) using different electrode arrays (panels b to d). The model consists of two blocks with resistivity values of 200 and 20 Ω.m buried in a 100 Ω.m background.

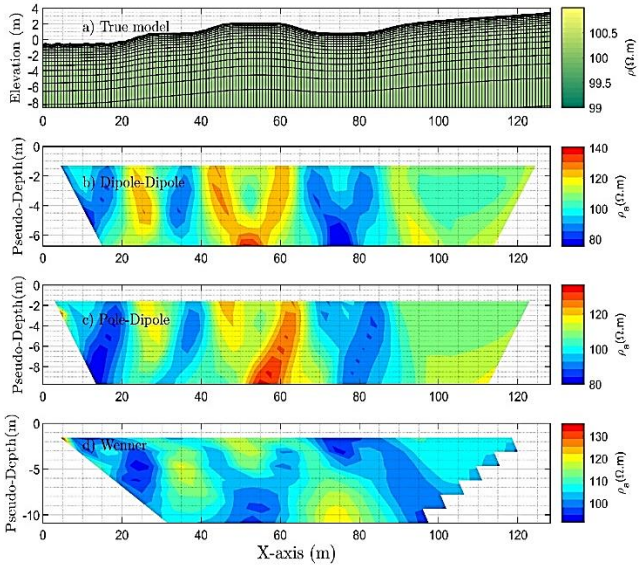

Figure 8. Apparent resistivity pseudo-sections computed by the proposed SC transformation method for Model 3 presented in panel (a) using different electrode arrays (panels b to d). The model is homogeneous at 100 Ω.m.

4. Conclusions

Whereas the effects of undulated surfaces in electrical resistance tomography measurements are inevitable, this paper has focused on developing and applying the direct Schwarz-Christoffel transformation method to incorporate topographical variations into the forward solver in the framework of the finite difference algorithm. The proposed mapping function is solved based on a numerical integration procedure. To numerically show the flexibility, reliability, and ease of use of the mapping function, we applied the proposed mapping function to a set of synthetic data examples derived from the most commonly used electrode configurations. The numerical results demonstrated that in the presence of topography; the simulated resistivity values do not

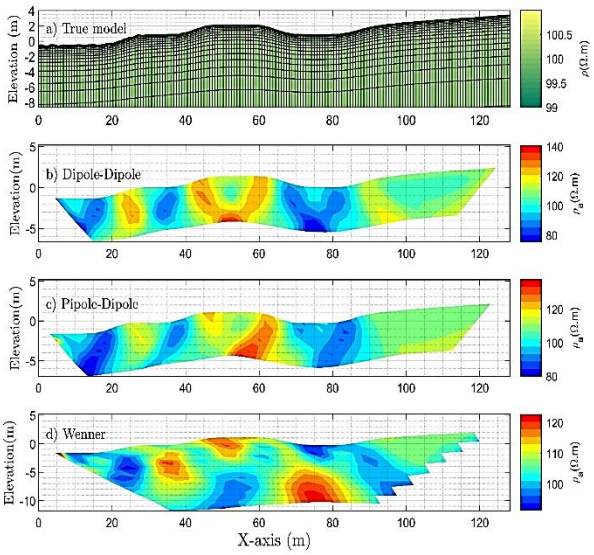

Figure 9. Apparent resistivity pseudo-sections computed by the commercial software RES2DMOD for Model 3 presented in panel (a) using different electrode arrays (panels b to d). The model is homogeneous at 100 $\Omega.m$.

reflect the true resistivity of the substructures even if the earth model has homogeneous resistivity distribution. The induced-terrain distortions in the measured resistivity values bring about unwanted conductive and resistive anomalies depending upon the type of configuration. It means that for the homogeneous model with a hill surface topography, the collinear Dipole-Dipole and Pole-Dipole arrays produce a high resistivity anomaly while the Wenner array leads to a conductive medium beneath the surface topography. In contrast, the data measured by the Dipole-Dipole and Pole-Dipole configurations in the presence of a valley surface topography show low resistivity values beneath the topography and the Wenner array produces an effect opposite to that of the Dipole-Dipole and Pole-Dipole resistivity data. In addition, we demonstrated that the effects of the conductive and resistive anomalies on the resistivity values are masked by the presence of undulating terrain tomography so that no discernible features of the subsurface anomalies were observed in the resistivity pseudo-sections. From the results presented in this study, one can conclude that the inverse solution of electrical resistance tomography with the incorporation of the topographical variations may cause a misleading image of the subsurface features. Due to the importance of the issue, in future work, we would deal with the effects of surface irregularities on the inversion of electrical resistance tomography data.

REFERENCES

[1] M. Loke, J. Chambers, D. Rucker, O. Kuras and P. Wilkinson, "Recent developments in the direct-current geoelectrical imaging method," Journal of Applied Geophysics, vol. 95, pp. 135-156, August 2013.

[2] T. Günther and T. Martin, "Spectral two-dimensional inversion of frequency-domain induced polarization data from a mining slag heap," Journal of Applied Geophysics, vol. 135, pp. 436-448, December 2016.

[3] A. F. Orozco, P. Ciampi, T. Katona, M. Censini, M. Petrangeli Papini, G. P. Deidda and G. Cassiani, "Delineation of hydrocarbon contaminants with multi-frequency complex conductivity imaging," Science of The Total Environment, vol. 768, 10 May 2021.

[4] M. Fallahsafari and R. Ghanati, "DC Electrical Resistance Tomography Inversion," Journal of the Earth and Space Physics, vol. 47, no. 4, pp. 87-98, 5 February 2022.

[5] C. Vachiratienchai, S. Boonchaisuk and W. Siripunvaraporn, "A hybrid finite difference–finite element method to incorporate topography for 2D direct current (DC) resistivity modeling," Physics of the Earth and Planetary Interiors, vol. 183, no. 3-4, pp. 426-434, December 2010.

[6] R. C. Fox, G. W. Hohmann, T. J. Killpack and L. Rijo, "Topographic effects in resistivity and induced - polarization surveys," Geophysics, vol. 45, no. 1, pp. 75-93, Jan 1980.

[7] T. H. Holcombe and G. R. Jiracek, "Three - dimensional terrain corrections in resistivity surveys," Geophysics, vol. 49, no. 4, pp. 439-452, Apr 1984.

[8] L. Tong and C. Yang, "Incorporation of topography into two - dimensional resistivity inversion," Geophysics, vol. 55, no. 3, pp. 354-361, Mar 1990.

[9] M.-J. Yi, J.-H. Kim, Y. Song, S.-J. Cho, S.-H. Chung and J.-H. Suh, "Three-dimensional imaging of subsurface structures using resistivity data," Geophysical Prospecting, vol. 49, no. 4, pp. 483-497, 2001.

[10] Z. Bing and S. A. Greenhalgh, "Finite element three dimensional direct current resistivity modelling: accuracy and efficiency considerations," Geophysical Journal International, vol. 145, no. 3, p. 679–688, June 2001.

[11] C. Rücker, T. Günther and K. Spitzer, "Three-dimensional modelling and inversion of dc resistivity data incorporating topography — I. Modelling," Geophysical Journal International, vol. 166, no. 2, p. 495–505, August 2006.

[12] M. Blome, H. Maurer and K. Schmidt , "Advances in three-dimensional geoelectric forward solver techniques," Geophysical Journal International, vol. 176, no. 3, p. 740–752, March 2009.

[13] Z. Ren and J. Tang, "3D direct current resistivity modeling with unstructured," Geophyssics, vol. 75, no. 1, p. H7–H17, 2010.

[14] S. Penz, H. Chauris, D. Donno and C. Mehl, "Resistivity modelling with topography," Geophysical Journal International, vol. 194, no. 3, p. 1486–1497, September 2013.

[15] E. Erdoğan, I. Demirci and M. E. Candansayar, "Incorporating topography into 2D resistivity modeling using finite-element and finite-difference approaches," Geophysics, vol. 73, no. 3, p. F135–F142, May 2008.

[16] I. Demirci, E. Erdoğan and M. E. Candansayar, "Two-dimensional inversion of direct current resistivity data incorporating topography by using finite difference techniques with triangle cells: Investigation of Kera fault zone in western Crete," Geophysics, vol. 77, no. 1, p. E67–E75, Jan 2012.

[17] R. Ghanati, Y. Azadi and R. Fakhimi, "RESIP2DMODE: A MATLAB-Based 2D Resistivity and Induced Polarization Forward Modeling Software," Iranian Journal of Geophysics, vol. 13, no. 4, pp. 60-78, February 2020.

[18] A. Dey and H. Morrison, "Resistivity modelling for arbitrarily shaped two-dimensional structures," Geophysical Prospecting, vol. 27, no. 1, pp. 106-136, March 1979.

[19] R. J. Spiegel, V. R. Sturdivant, and T. E. Owen, "Modeling resistivity anomalies from localized voids under irregular terrain," Geophysics, vol. 45, no. 7, pp. 1164-1183, Jul 1980.

[20] E. Costamagna, "On the Numerical Inversion of the Schwarz-Christoffel Conformal Transformation," IEEE Transactions on

Microwave Theory and Techniques, vol. 35, no. 1, pp. 35 - 40, January 1987.

[21] J. Chuang, Q. Gui and C. Hsiung, "Numerical computation of Schwarz-Christoffel transformation for simply connected unbounded domain," Computer Methods in Applied Mechanics and Engineering, vol. 105, no. 1, pp. 93-109, May 1993.

[22] M. Loke, "Geotomo software," 2019. [Online]. Available: http://geotomosoft.com/